Physics of Fluids

Electrohydrodynamic analysis of bubble burst in large Leidenfrost droplets

Cite as: Phys. Fluids **32**, 122002 (2020); https://doi.org/10.1063/5.0029106
Submitted: 10 September 2020 . Accepted: 04 November 2020 . Published Online: 02 December 2020

Onur Ozkan, and Vaibhav Bahadur

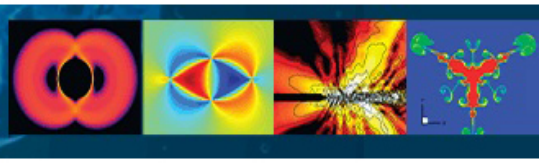

Physics of Fluids ARTICLE scitation.org/journal/phf

Electrohydrodynamic analysis of bubble burst in large Leidenfrost droplets

Cite as: Phys. Fluids 32, 122002 (2020); doi: 10.1063/5.0029106
Submitted: 10 September 2020 • Accepted: 4 November 2020 •
Published Online: 2 December 2020

Onur Ozkan and Vaibhav Bahadur[a)]

AFFILIATIONS

Walker Department of Mechanical Engineering, The University of Texas at Austin, Austin, Texas 78712, USA

[a)]Author to whom correspondence should be addressed: vb@austin.utexas.edu

ABSTRACT

A thin vapor gap forms underneath a liquid drop on a sufficiently hot surface, which prevents solid–liquid contact (the Leidenfrost effect). This vapor gap can be partly eliminated by applying an electrical potential difference across the vapor gap to electrostatically suppress the Leidenfrost state. An interesting hydrodynamics-related phenomenon that can occur in Leidenfrost droplets is the formation of a vapor dome and subsequent bubble burst at the center of the droplet. This work reports a comprehensive study of vapor dome formation and bubble burst in large Leidenfrost droplets under the influence of an electric field. First, a detailed numerical model (non-linear thin film lubrication equation) is developed to analyze the evolution of the vapor dome and bubble burst. Second, a simplified stability analysis is conducted to analytically estimate the critical droplet diameter (for bubble burst) under the influence of an electric field. Third, experiments are conducted to measure the critical diameter of Leidenfrost droplets for bubble burst under the influence of electric fields. The results from the numerical modeling and stability analysis show very good agreement with experimental measurements. The critical diameter for bubble burst and the time period between consecutive vapor bursts reduce with the applied electric field. Comparisons are made between the presently studied vapor burst and film boiling; similarity in the underlying hydrodynamic phenomena results in the length and time scales for bubble burst being similar to those encountered in film boiling.

I. INTRODUCTION

A volatile liquid droplet can be supported on its own vapor layer on sufficiently hot surfaces; this is known as the Leidenfrost effect and was first reported in 1756.[1] This phenomenon has been the subject of extensive theoretical and application-driven research. The insulating vapor layer between the surface and the liquid degrades boiling heat transfer significantly. This mode of boiling is called film boiling and is responsible for critical heat flux (CHF)-related restrictions on boiling heat transfer. Since this phenomen is encountered in several processes such as quenching of metals, microgravity applications, cooling of rocket nozzles, and nuclear reactor thermal management,[2,3] there have been significant efforts to increase the CHF and the Leidenfrost temperature.

Surface engineering[4–8] is a widely studied passive tool for CHF enhancement. Alternatively, active control and enhancement of heat transfer can be achieved via the application of electric fields to promote liquid-surface wetting, thereby suppressing the Leidenfrost state. There are multiple studies on electrostatic suppression of the Leidenfrost state in pool boiling configurations.[9–11] This study does not involve a pool boiling configuration but instead deals with large Leidenfrost droplets. The first study on the influence of electric fields on Leidenfrost droplets was by Takano *et al.*[12] and involved experiments and analysis of the critical voltage required for suppressing the Leidenfrost state in water and ethanol droplets.[13] Celestini and Kirstetter[14] visualized interference patterns below a Leidenfrost droplet with an electric field across the vapor gap to obtain insight into the nature of electrostatic suppression. The group under the corresponding author of this study has studied various aspects of electrostatic suppression including suppression at ultrahigh temperatures,[15] influence of the frequency of the AC waveform,[16] electrostatic suppression of the Leidenfrost state on liquid substrates,[17] acoustic detection of suppression,[18] electrical impedance-based characterization of suppression,[19] and heat transfer enhancement associated with electrostatic suppression.[20]

In addition to the heat transfer aspects, the hydrodynamics associated with Leidenfrost droplets has also received significant

attention. The shape of Leidenfrost droplets under various conditions has been extensively studied over the past decade. An accurate shape can be estimated by solving the thin film lubrication equation.[21,22] The vapor gap under a Leidenfrost droplet is larger near the center of the droplet as compared to the thickness near the edge.[21,22] The region of lowest vapor gap thickness is usually called the "neck." The difference between the vapor gap thickness near the center and the neck increases for larger droplets.[21,22] The thickness and shape of this vapor layer have been measured using analysis of diffraction patterns,[4] laser-light interference coupled with high-speed imaging,[23] high-speed color interferometry,[24] and x-ray imaging.[25,26] Moreover, the influence of the droplet size (from quasi-spherical to puddles)[3,21,22,27] and gravity[28] has been studied. Leidenfrost droplets on a heated liquid pool[29–31] and on a conical solid surface[32] have been looked at. The generation of vapor chimneys (eruption of the vapor dome) and the oscillation modes of Leidenfrost droplets on a conical surface[32] have been studied. Leidenfrost pattern formation (star-shaped patterns with different modes n = 0–16) and oscillations have been lately studied on a conical surface[32] and on flat surfaces.[33–36] Celestini *et al.*[37] studied the evaporation dynamics, droplet shape, hole nucleation, and oscillation modes in a Hele–Shaw cell. The liquid temporarily assumes a torus shape when the Leidenfrost drops are confined by a circular boundary because of the surface tension between the liquid and the circular body. The rotation and oscillation modes of Leidenfrost-levitated liquid tori have been experimentally and theoretically analyzed.[38,39]

It is noted that many of the above studies are motivated by an emerging suite of microfluidic applications involving the Leidenfrost state. These include spray cooling,[40–44] low friction droplet transportation,[45–54] Leidenfrost heat engine,[55] vibration isolation via Leidenfrost droplets,[56] vitrification of a liquid droplet on liquid nitrogen,[57] accelerated chemical reactions and organic synthesis,[58,59] green chemistry and nanofabrication in Leidenfrost drops,[60] removal of copper oxide layers,[61] and thin film fabrication using mist droplets.[62] Many of these microfluidic applications can benefit via the use of electric fields as a tool for droplet manipulation and heat transfer enhancement.

Leidenfrost droplets have a spherical or a semi-spherical shape as long as their diameter is smaller than or close to its capillary length. If the size of the Leidenfrost droplet is larger than a critical value, a vapor dome will form, grow, and eventually erupt as a result of Rayleigh–Taylor instability.[63] The critical size of the Leidenfrost droplet was measured and compared with predictions, based on the most unstable wavelength of the Rayleigh–Taylor instability.[63] In another study,[22] the maximum size of drops levitated by an "air cushion" is numerically estimated for different air flow rates through a porous substrate. Both studies mentioned in this paragraph suggest that the critical size of Leidenfrost droplets scales with the capillary length and is related to the wavelength of the Rayleigh–Taylor instability. Johnson[64] predicted that the most dominant wavelength in film (pool) boiling reduces under the influence of electric fields.

We note that vapor dome dynamics plays a significant role in wetting and heat transfer enhancement under electric fields as per a previous study.[19] Vapor dome formation in large Leidenfrost droplets limits the wetting area (thereby heat transfer enhancement) even under strong electric fields.[19] In recent years, there has been increasing interest in Leidenfrost droplets for multiple microfluidic and heat transfer applications. In any such study, the influence of vapor dome hydrodynamics underneath Leidenfrost droplets needs to be considered, especially for large droplets. We note that there is no existing study on vapor dome formation and vapor burst in Leidenfrost droplets under the influence of electric fields.

This study *analyzes vapor dome formation and bubble burst in large Leidenfrost droplets under the influence of an electric field*. In this study, a Leidenfrost droplet is considered to be "large" if its diameter is close to its critical value. Presently, the critical size of the Leidenfrost droplet and the vapor burst frequency are analyzed under the influence of electric fields. The critical diameter of the Leidenfrost droplet under the influence of electric fields is measured experimentally by high speed imaging. In addition to experimental measurements, the critical diameter is also estimated by numerical simulations and via a simplified stability analysis.

II. NUMERICAL FORMULATION OF VAPOR DOME FORMATION AND BUBBLE BURST

Film boiling is typically analyzed by solving the modified version of the Reynolds equation for Poiseuille flow.[21,22,65,66] Modeling the bottom part of a Leidenfrost droplet is very similar to modeling film boiling using the Reynolds equation. Figure 1 shows the shape of two Leidenfrost droplets with different sizes. The radius and the height of the droplets are scaled by the capillary length (l_c). The top part of the Leidenfrost droplet is modeled separately and the boundary conditions of both solutions need to be matched at a patching point,[21] as shown in Fig. 1. The droplet shape is assumed to be axisymmetric. The top and bottom parts of the numerical problem are shown in solid and dotted lines, respectively. The top part is solved by assuming a 180° contact angle with the ground, as shown

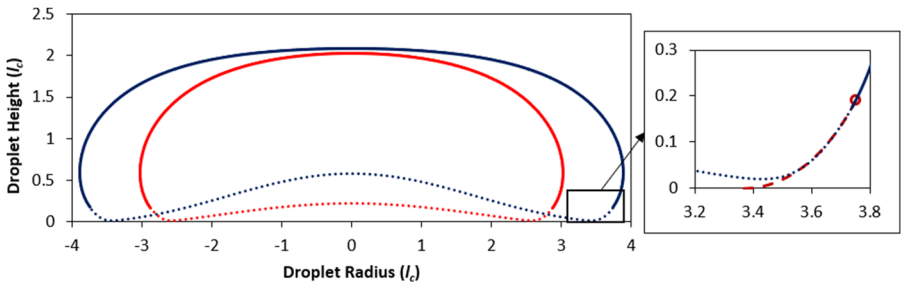

FIG. 1. Schematic showing the top and bottom parts of two Leidenfrost droplets (axisymmetric). Boundary conditions of the top and bottom parts are matched at the patching point.

by the red dashed line in the zoomed-in section of Fig. 1. We note that the focus of this study is on the shape and stability of the bottom part of the Leidenfrost droplet. Therefore, the solution of the top part is used as the boundary condition for the bottom part, as shown in Fig. 1. It is assumed that the shape of the top part remains the same.

Presently, the formulation proposed by Snoeijer *et al.*[22] was adopted for modeling the top part of the droplet (without making any changes),

$$\kappa + h = c, \tag{1}$$

where κ is the dimensionless curvature, h is the dimensionless height, and c is a constant. All length terms are scaled by the capillary length, $l_c = \sqrt{\sigma/\rho_l g}$, where σ is the surface tension, ρ_l is the liquid density, and g is the gravitational acceleration. The curvature has two principal components for a Leidenfrost droplet. The first component is shown in Fig. 1 on the r–z plane. The second component is due to the circular shape of the droplet from the top view. The radius of curvature for the second component is the radius normal to the surface ($r/\sin\theta$), where r is the radius in the z-plane and θ is the angle of the interface with the horizontal. The rest of the formulation for the top part of the droplet can be found in the work of Snoeijer *et al.*[22]

The solution of the top part of the droplet is combined with the bottom part solution by matching the boundary conditions at a patching point. A modified version of the Reynolds equation is used to account for the vapor mass flux due to evaporation as[65,66]

$$\frac{\partial h^*}{\partial t^*} = \frac{k_v \Delta T^*_{sup}}{\rho_v L h^*} + \frac{1}{12\mu_v}\nabla^*\left(h^{*3}\nabla^* P^*\right), \tag{2}$$

where k_v is the thermal conductivity of vapor, μ_v is the dynamic viscosity of vapor, ρ_v is the density of vapor, $\Delta\rho$ is the density difference between the liquid and the vapor, L is latent heat of evaporation, h^* is vapor gap thickness, t^* is time, ΔT^*_{sup} is superheat ($T^*_{surface} - T^*_{sat}$), and P^* is the film pressure. The asterisk ($*$) denotes unscaled variables (length, time, pressure, and temperature). Thermophysical properties are not scaled; however, they are shown without the asterisk ($*$). The length, time, and pressure scales used for non-dimensionalization are l_c, $\mu/gl_c\Delta\rho$, and $gl_c\Delta\rho$, respectively. The length scale is selected as the capillary length l_c instead of the mean initial vapor gap thickness. The time scale is obtained by dividing the length scale by the velocity scale ($gl_c^2\Delta\rho/g$). The pressure scale is selected as the hydrostatic pressure difference. It is noted that the pressure and time scales are selected as per the work of Panzarella *et al.*[66] The temperature is scaled by dividing the temperature by the saturation temperature, T^*_{sat}. After non-dimensionalization and rearrangements, the following non-dimensional Reynolds equation is obtained:

$$\frac{\partial h}{\partial t} = \frac{E\Delta T_{sup}}{h} + \frac{1}{12}\nabla\left(h^3\nabla P\right), \tag{3}$$

where h is the dimensionless film thickness, τ is the dimensionless time, ΔT_{sup} is the dimensionless superheat, and P is the dimensionless film pressure. E is the evaporation number, which is the ratio of viscous to evaporation time scales,

$$E = \frac{\mu_v k_v T^*_{sat}}{\rho_v \Delta\rho L g l_c^3}, \tag{4}$$

where T^*_{Sat} is the saturation temperature of the liquid.

Many studies[21,66] include only the influence of buoyancy and surface tension in the pressure term in Eq. (3). Panzarella *et al.*[66] solved initial value problems such as the collapse of an isothermal vapor film, growth of a vapor bubble in saturated film boiling, and the vapor film dynamics in subcooled film boiling. They derived the evolution equation that included the influence of van der Waals intermolecular forces and the vapor thrust (pressure jump across the free surface due to recoil of evaporating molecules). However, they did not provide any solutions but instead showed that the vapor thrust and van der Waals terms are small compared to the buoyancy term for typical film thicknesses in film boiling. We note that it is very reasonable to neglect vapor thrust and van der Waals interactions while modeling Leidenfrost droplets, since the vapor layer is relatively thick.[21,66] However, in the present situation, liquid wets the surface and vapor thrust and van der Waals interactions cannot be neglected.

The electrostatic pressure can be calculated as[14,15]

$$P^*_{el} = \frac{\varepsilon_{r,v}\varepsilon_0 V^2}{2h^{*2}}, \tag{5}$$

where $\varepsilon_{r,v}$ is the relative permittivity of vapor, ε_0 is the permittivity of free space, and V is the applied voltage. The electrostatic pressure in Eq. (5) can be non-dimensionalized by dividing by the pressure scale and replacing h^* by hl_c as

$$P_{el} = \frac{\varepsilon_{r,v}\varepsilon_0 V^2}{2g\Delta\rho l_c^3}\frac{1}{h^2} = El\frac{1}{h^2}. \tag{6}$$

The complete evolution equation for saturated boiling including the buoyancy, surface tension, vapor thrust, van der Waals force, and electrostatic force is

$$h_\tau = \frac{E\Delta T_{sup}}{h} - \frac{1}{12}\nabla\left[h^3\nabla\left(h + \kappa - \frac{A}{h^3} + \frac{(E\Delta T_{sup})^2 G}{h^2} - El\frac{1}{h^2}\right)\right]. \tag{7}$$

Equation (7) is the nondimensional form of Eq. (2) with the expanded pressure term in the parenthesis on the right-hand side. The terms in the inner parenthesis stand for (from left to right) buoyancy, surface tension, van der Waals, vapor thrust, and electrostatic forces. Non-dimensional terms A and G are the dimensionless Hamaker constant and modified Reynolds number,[66]

$$A = \frac{A^*}{6\pi\Delta\rho g l_c^4}, \tag{8}$$

where A^* is the Hamaker constant,

$$G = \frac{\rho_v \Delta\rho g l_c^3}{\mu_v^2}. \tag{9}$$

A similar equation was derived by Panzarella *et al.*[66] with two major differences. In this study, the lengths are scaled by the capillary length instead of the mean initial film thickness. Second, an electrostatic force is included in the analysis.

Equation (7) is numerically solved using the finite difference method with the Crank–Nicholson scheme without neglecting any terms. In order to deal with the solid–liquid contact numerically, the "disjoining pressure" term[67] is also added to the evolution equation as per

$$h_\tau = \frac{E\Delta T_{sup}}{h} - \frac{1}{12}\nabla\left[h^3\nabla\left(h + \kappa - \frac{A}{h^3} + \frac{(E\Delta T_{sup})^2 G}{h^2} - El\frac{1}{h^2} + \Pi\right)\right], \tag{10}$$

where Π is the disjoining pressure based on the two-term model,[67]

$$\Pi = \frac{(n-1)(m-1)}{h_{disj}(n-m)}(1-\cos\theta_e)\left(\left(\frac{h_{disj}}{h}\right)^n - \left(\frac{h_{disj}}{h}\right)^m\right), \tag{11}$$

where n and m are positive constants with $n > m > 1$ and θ_e is the contact angle. h_{disj} is the hypothetical film thickness in the contact region with $h_{disj} \ll h$. It is noted that the disjoining pressure term is negligible everywhere except in the vicinity of the contact region because h_{disj} is much smaller than h. Therefore, the disjoining pressure term is just a numerical trick to avoid a division by zero in Eq. (10).

We note that the formulation of the bottom part of the droplet builds up on the past work from Panzarella *et al.*[66] Presently, two new terms are added into the thin film lubrication equation: the electrostatic pressure in Eq. (5) and the disjoining pressure in Eq. (11) (to deal with the contact regions numerically). Another important difference is that the vapor thrust [Eq. (7)] and van der Walls [Eq. (7)] forces are not neglected in this study. Overall, this is the first study on detailed modeling of the shape of a Leidenfrost droplet under the influence of an electric field.

The relative magnitudes of the van der Waals, vapor thrust, and electrostatic forces with respect to the buoyancy term are shown in Fig. 2. A typical vapor layer thickness is 0.1 mm (0.04, when scaled by the capillary length of water). Therefore, the van der Waals and vapor thrust terms are negligible for a regular Leidenfrost droplet without electric fields according to Fig. 2.[66] However, the vapor layer thickness becomes smaller and partially zero under the influence of electric fields. Therefore, all terms in Eq. (10) need to be considered in the solid–liquid contact regions when simulating the electrical suppression of the Leidenfrost state.

Large Leidenfrost droplets (also called Leidenfrost puddles) are shown in Fig. 1 because this study focuses on the stability and vapor burst in large Leidenfrost droplets. Large Leidenfrost droplets (diameter > $5l_c$) have a flat shape rather than a quasi-spherical shape. It is noted that the lengths are scaled by the capillary length (2.5 mm for water). The droplet height does not increase much with the size of the droplet. The height of the vapor dome increases with the size of the Leidenfrost droplet. Figure 1 shows the steady-state solution of Eq. (10). The solution of Eq. (10) with the boundary conditions from the top part solution converges to a stable vapor dome shape if the droplet is smaller than its critical size. However, a steady state solution of Eq. (10) does not exist if the droplet size is larger than the critical size. In this case, the vapor dome keeps rising and grows above the droplet height, which results in vapor burst.

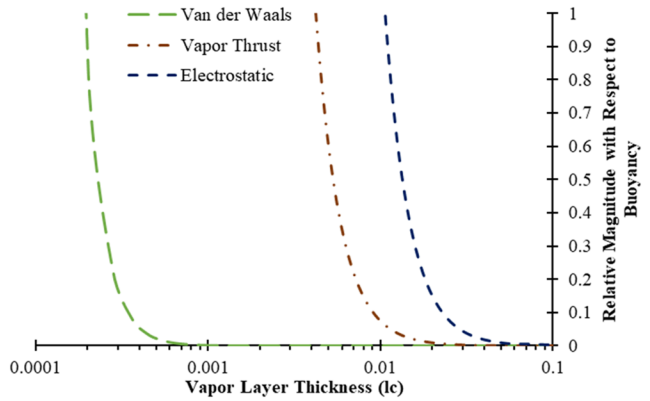

FIG. 2. Relative magnitude of van der Waals, vapor thrust, and electrostatic forces with respect to buoyancy vs the dimensionless vapor layer thickness (scaled by capillary length).

Figure 3 compares the results of simulations for Leidenfrost droplets without the electric field (El = 0) with the experimental measurements of Burton *et al.*,[23] where laser light interference was used for measuring the vapor gap profile under Leidenfrost droplets. Droplets with a radius larger than two capillary lengths are compared with experimental measurements. The largest stable droplet radius is 3.96 times the capillary length according to Fig. 3. When the droplet radius is increased to 3.97 times the capillary length, the numerical solution of the vapor dome did not have a steady solution below the height of the droplet. The simulation results show an excellent match with the measured data as per Fig. 3, which validates the numerical model for Leidenfrost droplets without an applied voltage. It is noted that prior experimental measurements of the vapor dome height under the influence of electric fields do not exist.

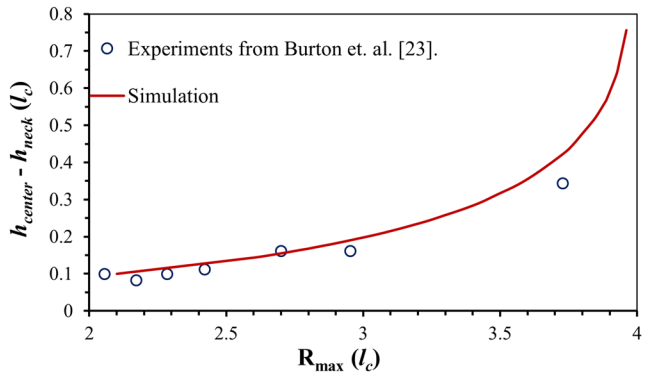

FIG. 3. Comparison of the center-to-neck height ($h_c - h_n$) with experimental measurements from Ref. 23. Solid line shows the results of the simulations [solving Eq. (10) with El = 0]. The vapor dome height and droplet radius are scaled by the capillary length, l_c.

III. ANALYSIS OF SIMPLIFIED RAYLEIGH–TAYLOR INSTABILITY

The critical diameter of a Leidenfrost droplet has been analytically estimated by Biance *et al.*[4] by analyzing the Rayleigh–Taylor instability of the lower interface. The critical diameter was calculated by evaluating the instability threshold of a small sinusoidal perturbation of magnitude ϵ. At equilibrium, the pressure must be the same at the center and neck of the droplet. The magnitude of the small perturbation, ϵ, cancels out when only capillary and gravitational effects are considered. Therefore, the critical radius depends on only the capillary length for Leidenfrost droplets in the absence of an external electric field. However, the same approach cannot be used for calculating the critical dimeter of a Leidenfrost droplet under the influence of an electric field because ϵ does not cancel out due to nonlinearities associated with the electrostatic pressure. In this study, a slightly different approach is adopted to deal with the nonlinearities and dependence of the critical radius on the initial perturbation.

A sinusoidal shape of the lower interface is assumed,

$$z = h_n + \frac{h_c}{2}\left(1 + \cos\frac{\pi}{R_n}r\right) \tag{12}$$

where h_n and h_c are the vapor layer thicknesses at the neck and center of the droplet, respectively, $h_c \gg h_n$, and R_n is the neck radius. Considering the capillary, gravitational, and electrostatic forces, the pressure difference between the center and the edge of the droplet is calculated as

$$\Delta P = \Delta P_c + \Delta P_g + \Delta P_e. \tag{13}$$

The terms on the right-hand side of Eq. (13) are pressures due to capillary, gravitational, and electrostatic forces, respectively, from left to right. The curvature of the lower interface is calculated as[21]

$$\kappa = \frac{z'' + \frac{1}{r}\left(1 + z''\right)z'}{\left(1 + z'^2\right)^{3/2}}. \tag{14}$$

The hydrostatic and capillary pressure are calculated at the center and the neck of the droplet. Their difference can be expressed as

$$\Delta P_c + \Delta P_g = 2\rho g\frac{h_c}{2}\left(1 - \frac{3}{2}\left(\frac{\pi l_c}{R}\right)^2\right), \tag{15}$$

where l_c is the capillary length. Equation (15) is the same equation as derived by Biance *et al.*[4] except for the perturbation magnitude, ϵ, being replaced by $h_c/2$ in this study. The electrostatic pressure is defined in Eq. (5) in the current study. Since $h_c \gg h_n$ and the electrostatic pressure is inversely proportional to the square of the distance h, the electrostatic pressure at the center of the droplet is negligible compared to the electrostatic pressure at the neck. Therefore, Eq. (13) becomes

$$\Delta P = 2\rho g\frac{h_c}{2}\left(1 - \frac{3}{2}\left(\frac{\pi l_c}{R}\right)^2\right) - \frac{\varepsilon_{r,v}\varepsilon_0 V^2}{2h_n^2}. \tag{16}$$

Equation (16) is equal to zero for a stable droplet. Therefore, the critical radius ($R = R_c$) can be calculated by solving Eq. (16) for R where $\Delta P = 0$ as

$$R_c = \frac{\pi l_c}{\sqrt{\frac{2}{3} + \frac{\varepsilon_{r,v}\varepsilon_0 V^2}{3\rho g h_n^2 h_c}}}. \tag{17}$$

The maximum stable radius of a given droplet is calculated by using Eq. (17) for a given height of the vapor dome at the center and in the neck region. A stable droplet (without vapor burst) must have a dome height that is smaller than the height of the droplet. Therefore, the h_c term can be replaced by droplet height, which is equal to twice the capillary length,[4] assuming that it does not change with the applied voltage. The height of the vapor layer at the droplet neck is ~100 μm for a large water droplet on a 300 °C surface. The critical radius in Eq. (17) is compared with the critical radius estimation in the numerical simulations and subsequently described experimental measurements. Finally, it is noted that the critical radius in Eq. (17) reduces to $R_c = 3.84l_c$ when the applied voltage is zero, which is the same as the one reported by Biance *et al.*[4]

IV. DESCRIPTION OF EXPERIMENTS

The minimum size of a Leidenfrost droplet (under the influence of an electric field) that can sustain vapor burst is experimentally determined. A schematic of the experimental setup and two snapshots from high-speed visualization are shown in Fig. 4. A thin, stainless steel ring is used to contain the cylindrical droplet and to apply the voltage. Retaining rings of different sizes are used for various electric fields. High-speed videos (>1000 fps) are recorded from the top. The minimum diameter of the droplet (decided by the retaining ring) that can sustain vapor burst is recorded as the critical diameter of the Leidenfrost droplet. The volume of a free Leidenfrost droplet for a given diameter (without a retaining ring) is calculated

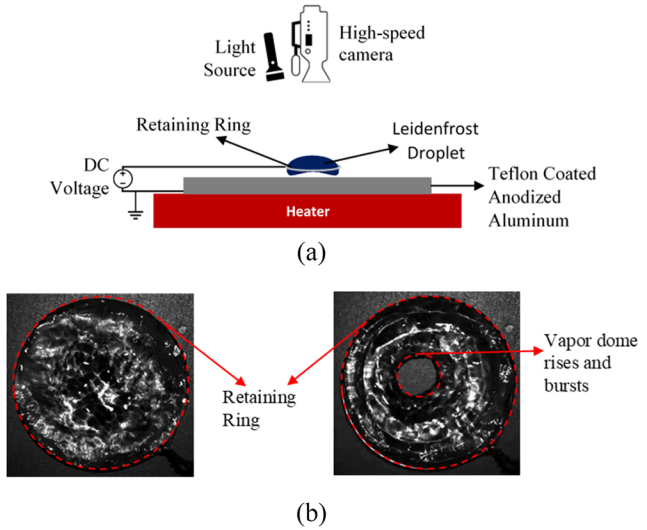

FIG. 4. (a) Schematic of the experimental setup. (b) Top view of Leidenfrost droplets. The left image shows the Leidenfrost droplet before the rise of the vapor dome. The right image shows the droplet during vapor burst.

numerically and is dispensed to ensure that the distortion of the droplet due to the retaining ring is minimized. The same diameter of the droplet can be sustained with different volumes because of the surface tension between the retaining ring and the liquid. This would result in a distorted shape of the droplet. The risk of droplet shape distortion is minimized by dispensing the appropriate volume of liquid for a given diameter.

The Leidenfrost droplet temporarily becomes a torus-like body after the vapor dome bursts, as shown in the second image in Fig. 4(b). The vapor pressure under the droplet reduces due to mass loss after the vapor burst, so the droplet cannot maintain its torus shape and quickly returns to its original shape. All of this is seen clearly in the videos included in the supplementary material. Our previous study[19] showed that the wetting fraction is limited by a number that is smaller than one since complete wetting is not possible due to perpetual evaporation. This limiting wetting fraction reduces for larger droplets due to the vapor dome formation underneath the droplet.

The height of the vapor dome (h_{center}) increases sharply with the size of the Leidenfrost droplet according to Figs. 1 and 3. If the diameter of the droplet is larger than a critical value, the vapor dome grows above the height of the droplet and vapor burst is observed. The experiments start with a retaining ring (or droplet diameter) that is smaller than the critical diameter, where vapor burst is not observed. Next, the diameter of the retaining ring and the Leidenfrost droplet is gradually increased until the vapor dome and burst are observed from the top view of the droplet. The minimum diameter of the Leidenfrost droplet that can sustain vapor burst is noted as the critical size for that particular electric field. The same procedure is repeated at multiple values of the applied voltage.

V. RESULTS AND DISCUSSIONS

Figure 5 (Multimedia view) shows snapshots of deionized water (DI) Leidenfrost droplets (or puddles). No voltage is applied to the droplet shown in Fig. 5(a) (Multimedia view), whereas 150 V is applied to the droplet in Fig. 5(b) (Multimedia view). The droplet diameters in Figs. 5(a) and 5(b) (Multimedia view) are 21.9 mm and 19.1 mm, respectively. The physics underlying the vapor dome rise and burst is the Rayleigh–Taylor instability (due to the low density vapor layer under high density liquid). Since the same physics governs vapor dome rise (and bubble burst) and film boiling, the critical diameter of the Leidenfrost droplet can be compared with the wavelength of the most unstable oscillation in pool film boiling. The most unstable wavelength of the Rayleigh–Taylor instability in film boiling is[2]

$$\lambda_c = 2\pi\sqrt{\frac{3\sigma}{\Delta\rho g}} = 2\sqrt{3}\pi l_c. \tag{18}$$

The capillary length (l_c) for water is 2.5 mm. According to Eq. (18), the wavelength of the most unstable wavelength in film boiling is 27.2 mm for water. It is expected that the critical size

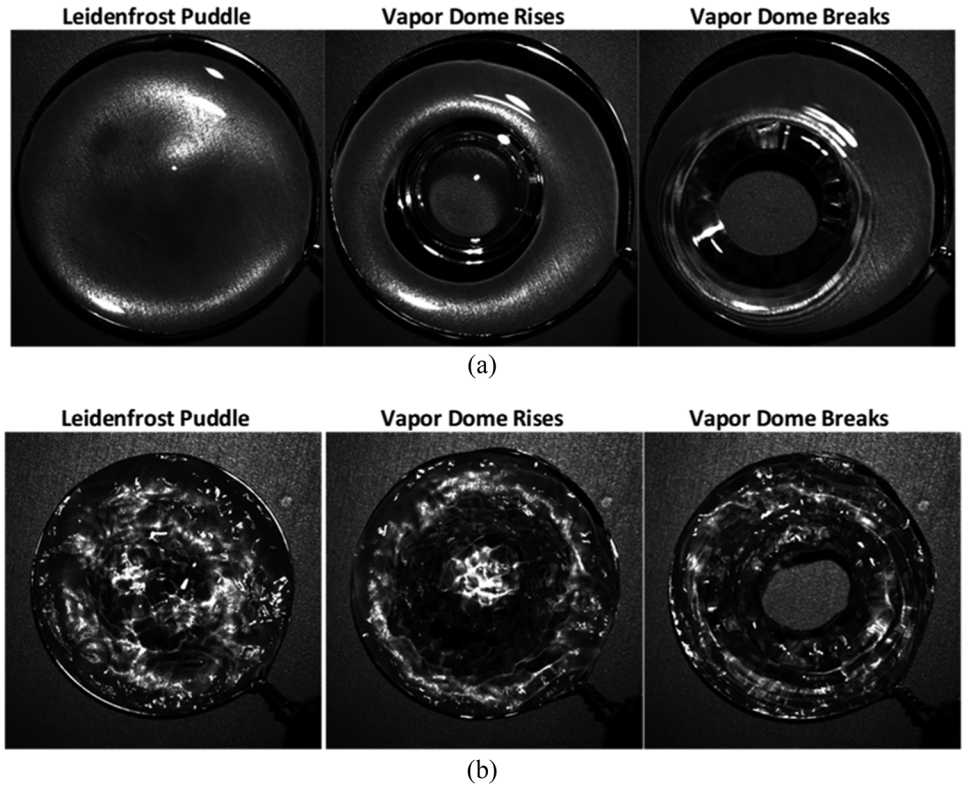

FIG. 5. High-speed visualization snapshots of water Leidenfrost droplets. (a) No voltage is applied. The vapor dome rises at the center (center image) and then bursts (right image). (b) Applied voltage: 150 V. The vapor dome is not visible from the top (center image) because of the instabilities on the liquid surface due to Leidenfrost suppression. Vapor burst is seen in the right image. See the supplementary material for videos showing the top view of Leidenfrost droplets (depicting the vapor dome rise and bubble burst) at no voltage and 150 V. Multimedia views: https://doi.org/10.1063/5.0029106.1; https://doi.org/10.1063/5.0029106.2

of the Leidenfrost droplet will scale with the capillary length. It is noted that there are also some fundamental differences between the stability of pool film boiling and a Leidenfrost droplet. The critical diameter of a Leidenfrost droplet has been analytically calculated by Biance *et al.*[4] using stability analysis as

$$D_c = 7.68 l_c. \tag{19}$$

Equation (19) was derived for a Leidenfrost droplet, so it is expected to have a better match with the current experimental measurement compared to λ_c in Eq. (18). The critical diameter of a water Leidenfrost drop is 19.2 mm according to Eq. (19). The critical diameter of the Leidenfrost droplet was measured to be 21.9 mm in the current study, which is ~15% larger than the estimation from Eq. (19). Also, the critical diameter is 19.9 mm according to our numerical analysis (Fig. 3). There is thus an excellent match between numerical simulations and stability analysis [Eq. (19)]. Another comparison can be made with the work of Snoeijer *et al.*[22] where the critical radius was reported as ~3.95 times the capillary length, which is 19.9 mm for a water droplet.

The 15% difference between the experimental measurements and the numerical simulations can be attributed to the retaining ring used in the current study and its hydrodynamic effects on the Leidenfrost droplet. The retaining ring is used to control size of the drop. However, its purpose is also to enable the application of an electric field in the vapor gap and keep the droplet in place. Strong electric fields can significantly reduce the vapor layer and lead to partial wetting on the hot surface, which will result in evaporation-induced pressure buildup. Droplets (especially large ones) tend to move and spin around the electrode and even escape. Therefore, a retaining ring is essential to keep the droplet attached to the electrode and maintain a steady, circular shape.

Figure 5 (Multimedia view) shows the smallest diameters at which the droplets become unstable and vapor bursts are observed. The diameter of the retaining ring and the droplet is increased step-by-step until vapor bursts are observed. According to Fig. 5 (Multimedia view), the critical diameter of a Leidenfrost droplet decreases with the electric field. This is expected and can be explained by the similarities in the rise of the vapor dome in a Leidenfrost droplet and the most unstable oscillation in pool film boiling. The wavelength of the most unstable oscillation in film boiling reduces with the applied voltage[9] due to increased boiling rate and vapor generation. Although a decrease in the critical diameter of Leidenfrost droplets should be an expected outcome of applying electric fields, it has neither been demonstrated nor analyzed in any literature studies.

Figure 6 shows the steady-state shape of Leidenfrost droplets smaller than the critical size (solid lines) and the unsteady evolution of the vapor gap in Leidenfrost droplets larger than the critical size (dashed lines). Figure 6(a) shows the shapes of two Leidenfrost droplets that are slightly smaller and larger than their critical sizes without an electric field. The droplet has a steady-state shape when its radius is smaller than 3.97 capillary lengths [Fig. 6(a)]. Equation (10) does not have a steady-state solution when the droplet is larger the critical diameter ($3.97 l_c$). The large droplet shown in Fig. 6(a) is slightly larger than its critical size, so it does not have a

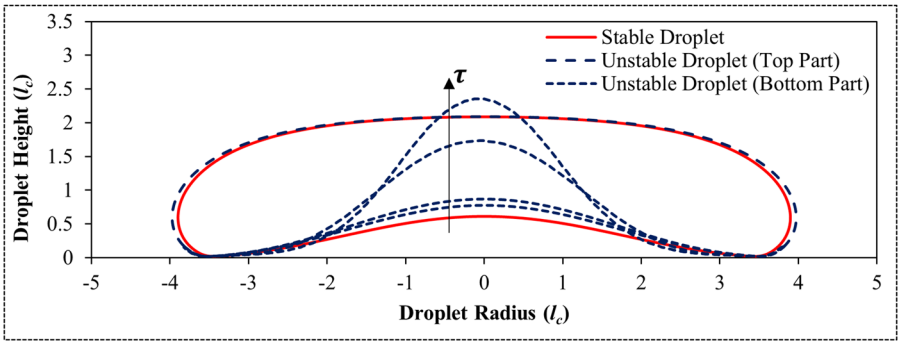

(a)

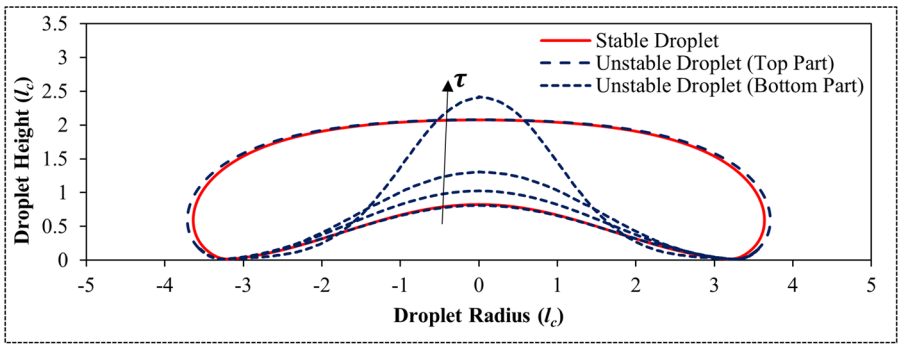

(b)

FIG. 6. Numerical simulation of Leidenfrost droplets of sizes near the critical diameter ($R_c = 3.97 l_c$) (a) without an electric field. Smaller droplet has a stable shape (red solid line). Larger droplet does not have a stable shape (blue dashed line) (b) with 100 V applied. Smaller droplet has a stable shape (red solid line). Larger droplet does not have a stable shape (blue dashed line). The vapor dome height and droplet radius are scaled by the capillary length, l_c.

steady-state shape. The simulation starts from the bottom dashed line and the vapor dome grows continuously with the simulation time (τ), as shown in Fig. 6(a). The vapor dome keeps rising above the height of the droplet, which suggests that bubble burst will happen. The current numerical model is not meant to handle vapor burst; therefore, the simulation is terminated when the vapor dome grows above the height of the droplet.

Figure 6(b) shows the shape of Leidenfrost droplets that are slightly smaller and larger than the critical size under the influence of an electric field. The droplet is assumed to be equipotential at 100 V and the bottom surface is grounded. Similar to Fig. 6(a), the droplet in Fig. 6(b) does not have a steady-state shape when the diameter is larger than the critical diameter. It is noted that the critical size of the droplet is 8% smaller in Fig. 6(b) compared to Fig. 6(a) due to the applied electric field.

Figure 7 shows the height of the vapor dome as a function of the droplet size and the applied voltage. The height increases exponentially as the droplet size approaches its critical size. It is noted that vapor dome height curves are cut before their critical size because there is no steady-state solution beyond this point. The height of the vapor dome increases under the influence of an electric field. As the applied voltage is increased, the steady-state height of the vapor dome increases and the critical size of the Leidenfrost droplet decreases.

Next, the critical diameter of the Leidenfrost droplet under the influence of an electric field ($D_{crit,V}$) is normalized by the critical diameter without an electric field ($D_{crit,0}$) and is shown in Fig. 8. The critical diameter reduces with the applied voltage as per experimental measurements and numerical simulations. A 20% reduction in the critical diameter is experimentally measured at 175 V (Fig. 8). The numerical simulation captures the trend very well, albeit with slightly lower values than experimental measurements. This can be attributed to the retaining ring. For smaller droplets, the circumference to area (or circumference to volume) ratio increases. Therefore, the surface tension between the retaining ring and the liquid becomes more important for lower droplet sizes.

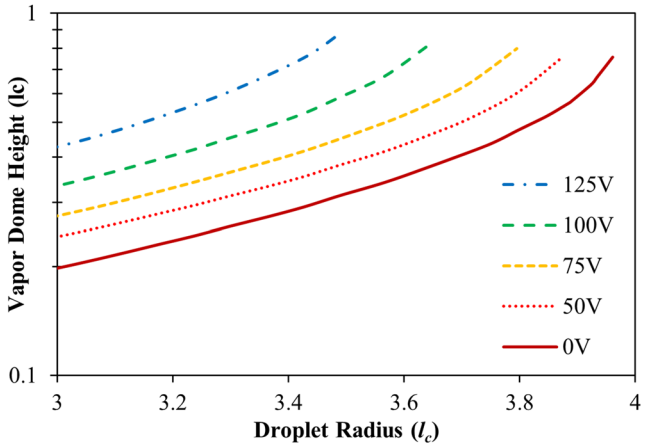

FIG. 7. Dependence of the vapor dome height on the size of Leidenfrost droplets under various applied voltages. The vapor dome height and droplet radius are scaled by the capillary length, l_c.

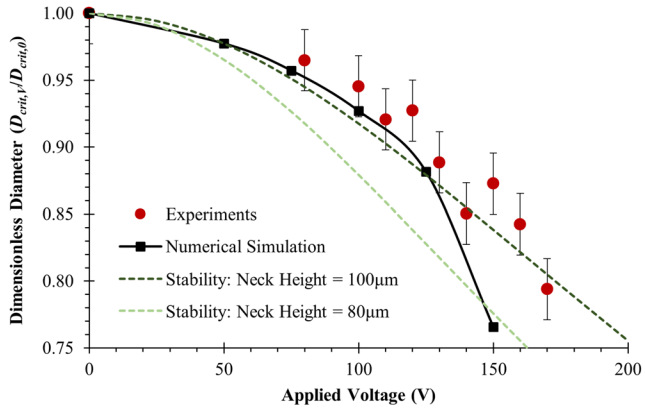

FIG. 8. Normalized critical diameter of the Leidenfrost droplets vs the applied voltage. Experimental measurements for water droplets are compared with simulations and stability analysis.

The critical diameter, as calculated by Eq. (17) is plotted in Fig. 8 for two different neck height values. The neck height is ~100 μm for a large water Leidenfrost droplet without an applied voltage.[4] This explains the match between the numerical simulations and the stability analysis with the 100 μm neck height. It is noted that the diameter is slightly lower than experimental values in the low voltage region, since the influence of the retaining ring on hydrodynamics was ignored. In the higher voltage region, the stability analysis with a smaller neck height (80 μm) matches the numerical simulations better than analysis with a 100 μm neck height. The reason is that the mean neck height reduces at higher voltages due to the increased liquid-surface electrostatic attraction. We note that the uncertainty in measuring the critical diameter is 0.5 mm.

In addition to the influence of the electric field on the critical diameter of the droplet, the time period between consecutive vapor bursts is also a parameter of interest. It is noted that the time period between consecutive vapor bubbles in film boiling reduces with an electric field.[9] Figure 9 shows the time period between consecutive vapor bursts for water droplets under an applied voltage.

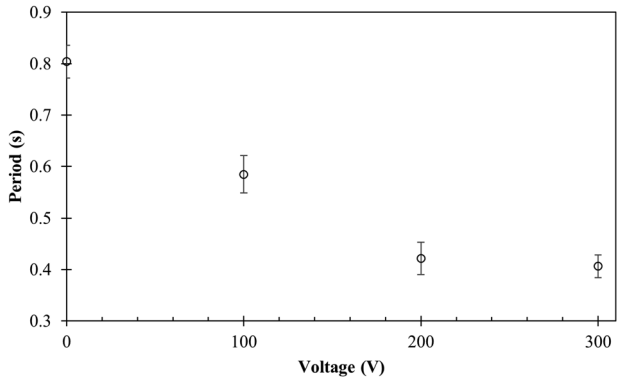

FIG. 9. Average time period between consecutive vapor bursts vs the applied voltage for water droplets.

The measured average time period between two consecutive vapor bursts is 0.8 s in the absence of an applied voltage. The average time period of oscillations reduces under the influence of an electric field in pool film boiling[9] because of the enhanced evaporation rate due to the suppression of the Leidenfrost state. Analogously, a reduction in the vapor burst period is observed for Leidenfrost droplets under the influence of electric fields, as per Fig. 9. The time period between two consecutive vapor bursts is reduced by 50% for an applied voltage of 200 V.

VI. CONCLUSIONS

Overall, this study examines the hydrodynamics, stability, and bubble burst in Leidenfrost droplets under the influence of electric fields. We show that vapor dome formation is a significant hydrodynamic phenomenon that influences the wetting dynamics (and consequently the heat transfer) during electrostatic suppression of the Leidenfrost state. The vapor dome under a Leidenfrost droplet grows and bubble burst occurs for Leidenfrost droplets above a critical diameter. This critical diameter reduces with an applied potential difference across the vapor gap. The evolution of the vapor dome and bubble burst is studied via fundamental analysis (of the Rayleigh–Taylor instability), numerical simulations (thin film lubrication equation with non-linear terms included), and experiments (high speed visualization of bubble burst). Results show that the critical diameter for bubble burst and the time period between consecutive vapor bursts reduces with the applied electric field.

ACKNOWLEDGMENTS

The authors acknowledge the National Science Foundation (Grant No. CBET-1605789) for supporting this work. The authors also acknowledge a research Award from Google, and the UT Austin Portugal program for partial support of this work.

DATA AVAILABILITY

The data that support the findings of this study are available from the corresponding author upon reasonable request.

REFERENCES

[1]J. G. Leidenfrost, "On the fixation of water in diverse fire," Int. J. Heat Mass Transfer **9**, 1153–1166 (1966).
[2]N. Zuber and M. Tribus, "Further remarks on the stability of boiling heat transfer," Report 58-5, Project 35, AECU-3631, United States Atomic Energy Commission.
[3]X. Xu and T. Qian, "Hydrodynamics of Leidenfrost droplets in one-component fluids," Phys. Rev. E **87**(4), 043013 (2013).
[4]A.-L. Biance, C. Clanet, and D. Quéré, "Leidenfrost drops," Phys. Fluids **15**(6), 1632–1637 (2003).
[5]C. M. Kunkle and V. P. Carey, "Metrics for quantifying surface wetting effects on vaporization processes at nanostructured hydrophilic surfaces," in Proceedings of the ASME 2016 Heat Transfer Summer Conference, 2016.
[6]J. D. Bernardin and I. Mudawar, "The Leidenfrost point: Experimental study and assessment of existing models," J. Heat Transfer **121**, 894–903 (1999).
[7]H. O'Hanley *et al.*, "Separate effects of surface roughness, wettability, and porosity on the boiling critical heat flux," Appl. Phys. Lett. **103**(2), 024102 (2013).
[8]I. U. Vakarelski *et al.*, "Stabilization of Leidenfrost vapour layer by textured superhydrophobic surfaces," Nature **489**(7415), 274–277 (2012).
[9]T. B. Jones, "Electrohydrodynamically enhanced heat transfer in liquids: A review," Adv. Heat Transfer **14**, 107–148 (1979).
[10]P. H. G. Allen and T. G. Karayiannis, "Electrohydrodynamic enhancement of heat transfer and fluid flow," Heat Recovery Syst. CHP **15**(5), 389–423 (1995).
[11]S. Laohalertdecha, P. Naphon, and S. Wongwises, "A review of electrohydrodynamic enhancement of heat transfer," Renewable Sustainable Energy Rev. **11**(5), 858–876 (2007).
[12]K. Takano, I. Tanasawa, and S. Nishio, "Enhancement of evaporation of a liquid droplet using EHD effect: Criteria for instability of gas-liquid interface under electric field," J. Enhanc. Heat Transfer **3**(1), 73–81 (1996).
[13]K. Takano, I. Tanasawa, and S. Nishio, "Enhancement of evaporation of a droplet using EHD effect. Onset of instability of gas-liquid interface under electric field applied in a stepwise manner," JSME Int. J. **38**(2), 288–294 (1995).
[14]F. Celestini and G. Kirstetter, "Effect of an electric field on a Leidenfrost droplet," Soft Matter **8**(22), 5992 (2012).
[15]A. Shahriari, J. Wurz, and V. Bahadur, "Heat transfer enhancement accompanying Leidenfrost state suppression at ultrahigh temperatures," Langmuir **30**(40), 12074–12081 (2014).
[16]O. Ozkan, A. Shahriari, and V. Bahadur, "Electrostatic suppression of the Leidenfrost state using AC electric fields," Appl. Phys. Lett. **111**(14), 141608 (2017).
[17]A. Shahriari, O. Ozkan, and V. Bahadur, "Electrostatic suppression of the leidenfrost state on liquid substrates," Langmuir **33**(46), 13207–13213 (2017).
[18]A. Shahriari, P. S. Wilson, and V. Bahadur, "Acoustic detection of electrostatic suppression of the Leidenfrost state," Phys. Rev. E **98**, 013103 (2018).
[19]O. Ozkan and V. Bahadur, "Electrical impedance-based characterization of electrostatic suppression of the Leidenfrost state," Appl. Phys. Lett. **114**, 153701 (2019).
[20]O. Ozkan and V. Bahadur, "Heat transfer enhancement associated with electrostatic suppression of Leidenfrost droplets," Int. J. Heat Mass Transfer **149**, 119207 (2020).
[21]B. Sobac, A. Rednikov, S. Dorbolo, and P. Colinet, "Leidenfrost effect: Accurate drop shape modeling and refined scaling laws," Phys. Rev. E **90**(5), 053011 (2014).
[22]J. H. Snoeijer, P. Brunet, and J. Eggers, "Maximum size of drops levitated by an air cushion," Phys. Rev. E **79**(3), 036307 (2009).
[23]J. C. Burton, A. L. Sharpe, R. C. A. van der Veen, A. Franco, and S. R. Nagel, "Geometry of the vapor layer under a Leidenfrost drop," Phys. Rev. Lett. **109**(7), 074301 (2012).
[24]R. C. A. van der Veen, T. Tran, D. Lohse, and C. Sun, "Direct measurements of air layer profiles under impacting droplets using high-speed color interferometry," Phys. Rev. E **85**(2), 026315 (2012).
[25]G. C. Lee *et al.*, "Measurement of the vapor layer under a dynamic Leidenfrost drop," Int. J. Heat Mass Transfer **124**, 1163–1171 (2018).
[26]P. R. Jones *et al.*, "High-speed X-ray imaging of the Leidenfrost collapse," Sci. Rep. **9**, 1598 (2019).
[27]Y. Pomeau, M. Le Berre, F. Celestini, and T. Frisch, "The Leidenfrost effect: From quasi-spherical droplets to puddles," C. R. Mech. **340**(11-12), 867–881 (2012).
[28]L. Maquet, M. Brandenbourger, B. Sobac, A. L. Biance, P. Colinet, and S. Dorbolo, "Leidenfrost drops: Effect of gravity," EPL (Europhys. Lett.) **110**(2), 24001 (2015).
[29]L. Maquet *et al.*, "Leidenfrost drops on a heated liquid pool," Phys. Rev. Fluids **1**(5), 053902 (2016).
[30]L. Qiao, Z. Zeng, H. Xie, H. Liu, and L. Zhang, "Modeling Leidenfrost drops over heated liquid substrates," Int. J. Heat Mass Transfer **128**, 1296–1306 (2019).
[31]C. Y. H. Wong, M. Adda-Bedia, and D. Vella, "Non-wetting drops at liquid interfaces: From liquid marbles to Leidenfrost drops," Soft Matter **13**(31), 5250–5260 (2017).
[32]S. Hidalgo-Caballero, Y. Escobar-Ortega, and F. Pacheco-Vázquez, "Leidenfrost phenomenon on conical surfaces," Phys. Rev. Fluids **1**(5), 051902 (2016).
[33]P. Prabhakaran, A. Krekhov, E. Bodenschatz, and S. Weiss, "Leidenfrost pattern formation and boiling," J. Stat. Phys. **175**(3-4), 598–616 (2019).
[34]X. Ma, J. J. Liétor-Santos, and J. C. Burton, "Star-shaped oscillations of Leidenfrost drops," Phys. Rev. Fluids **2**(3), 031602 (2017).

[35]G. Paul, P. K. Das, and I. Manna, "Droplet oscillation and pattern formation during Leidenfrost phenomenon," Exp. Therm. Fluid Sci. **60**, 346–353 (2015).
[36]X. Ma and J. C. Burton, "Self-organized oscillations of Leidenfrost drops," J. Fluid Mech. **846**, 263–291 (2018).
[37]F. Celestini, T. Frisch, A. Cohen, C. Raufaste, L. Duchemin, and Y. Pomeau, "Two dimensional Leidenfrost droplets in a Hele-Shaw cell," Phys. Fluids **26**(3), 032103 (2014).
[38]A. Ludu and A. Raghavendra, "Rotating hollow patterns in fluids," Appl. Numer. Math. **141**, 167–184 (2019).
[39]S. Perrard, Y. Couder, E. Fort, and L. Limat, "Leidenfrost levitated liquid tori," EPL (Europhys. Lett.) **100**(5), 54006 (2012).
[40]H. Chen, W.-l. Cheng, Y.-h. Peng, and L.-j. Jiang, "Dynamic Leidenfrost temperature increase of impacting droplets containing high-alcohol surfactant," Int. J. Heat Mass Transfer **118**, 1160–1168 (2018).
[41]S. Huang, S. Yin, F. Chen, H. Luo, Q. Tang, and J. Song, "Directional transport of droplets on wettability patterns at high temperature," Appl. Surf. Sci. **428**, 432–438 (2018).
[42]C. E. Clavijo, J. Crockett, and D. Maynes, "Hydrodynamics of droplet impingement on hot surfaces of varying wettability," Int. J. Heat Mass Transfer **108**, 1714–1726 (2017).
[43]M. A. J. Van Limbeek, M. Shirota, P. Sleutel, C. Sun, A. Prosperetti, and D. Lohse, "Vapour cooling of poorly conducting hot substrates increases the dynamic Leidenfrost temperature," Int. J. Heat Mass Transfer **97**, 101–109 (2016).
[44]M. Gradeck, N. Seiler, P. Ruyer, and D. Maillet, "Heat transfer for Leidenfrost drops bouncing onto a hot surface," Exp. Therm. Fluid Sci. **47**, 14–25 (2013).
[45]G. Lagubeau, M. Le Merrer, C. Clanet, and D. Quéré, "Leidenfrost on a ratchet," Nat. Phys. **7**(5), 395–398 (2011).
[46]A. Würger, "Leidenfrost gas ratchets driven by thermal creep," Phys. Rev. Lett. **107**(16), 164502 (2011).
[47]J. T. Ok, J. Choi, E. Brown, and S. Park, "Effect of different fluids on rectified motion of Leidenfrost droplets on micro/sub-micron ratchets," Microelectron. Eng. **158**, 130–134 (2016).
[48]H. Linke *et al.*, "Self-propelled Leidenfrost droplets," Phys. Rev. Lett. **96**(15), 154502 (2006).
[49]J. T. Ok, E. Lopez-Oña, D. E. Nikitopoulos, H. Wong, and S. Park, "Propulsion of droplets on micro- and sub-micron ratchet surfaces in the Leidenfrost temperature regime," Microfluidics Nanofluidics **10**(5), 1045–1054 (2011).
[50]A. Grounds, R. Still, and K. Takashina, "Enhanced droplet control by transition boiling," Sci. Rep. **2**, 720 (2012).
[51]M.-y. Chen, Z.-h. Jia, T. Zhang, and Y.-y. Fei, "Self-propulsion of Leidenfrost droplets on micropillared hot surfaces with gradient wettability," Appl. Surf. Sci. **433**, 336–340 (2018).
[52]P. Yi *et al.*, "Oscillation and self-propulsion of Leidenfrost droplets enclosed in cylindrical cavities," Soft Matter **310**(2), 8854–8860 (2020).
[53]J. Li *et al.*, "Rectification of mobile Leidenfrost droplets by planar ratchets," Small **16**(9), 1901751 (2020).
[54]A. Bouillant, T. Mouterde, P. Bourrianne, A. Lagarde, C. Clanet, and D. Quéré, "Leidenfrost wheels," Nat. Phys. **14**(12), 1188–1192 (2018).
[55]P. Agrawal *et al.*, "Leidenfrost heat engine: Sustained rotation of levitating rotors on turbine-inspired substrates," Appl. Energy **240**, 399–408 (2019).
[56]B. T. Ng, Y. M. Hung, and M. K. Tan, "Vibration isolation via Leidenfrost droplets," J. Micromech. Microeng. **29**(8), 085003 (2019).
[57]Y. S. Song *et al.*, "Vitrification and levitation of a liquid droplet on liquid nitrogen," Proc. Natl. Acad. Sci. U. S. A. **107**(10), 4596–4600 (2010).
[58]R. M. Bain, C. J. Pulliam, F. Thery, and R. G. Cooks, "Accelerated chemical reactions and organic synthesis in leidenfrost droplets," Angew. Chem., Int. Ed. **55**(35), 10478–10482 (2016).
[59]M. Abdelaziz *et al.*, "Transflective mesoscopic nanoparticles synthesized in the Leidenfrost droplet as black absorbers," Adv. Mater. Interfaces **6**(1), 1801610 (2019).
[60]R. Abdelaziz *et al.*, "Green chemistry and nanofabrication in a levitated Leidenfrost drop," Nat. Commun. **4**, 2400 (2013).
[61]C. Raufaste, Y. Bouret, and F. Celestini, "Reactive Leidenfrost droplets," EPL (Europhys. Lett.) **114**(4), 46005 (2016).
[62]T. Kawaharamura, "Physics on development of open-air atmospheric pressure thin film fabrication technique using mist droplets: Control of precursor flow," Jpn. J. Appl. Phys., Part 1 **53**, 05FF08 (2014).
[63]G. Paul, I. Manna, and P. Kumar Das, "Formation, growth, and eruption cycle of vapor domes beneath a liquid puddle during Leidenfrost phenomena," Appl. Phys. Lett. **103**(8), 084101 (2013).
[64]R. L. Johnson, "Effect of an electric field on boiling heat transfer," AIAA J. **6**(8), 1456–1460 (1968).
[65]J. P. Burelbach, S. G. Bankoff, and S. H. Davis, "Nonlinear stability of evaporating/condensing liquid films," J. Fluid Mech. **195**, 463 (1988).
[66]C. H. Panzarella, S. H. Davis, and S. G. Bankoff, "Nonlinear dynamics in horizontal film boiling," J. Fluid Mech. **402**, 163–194 (2000).
[67]L. W. Schwartz, "Hysteretic effects in droplet motions on heterogeneous substrates: Direct numerical simulation," Langmuir **14**(12), 3440–3453 (1998).